

NANO · MICRO
small

Supporting Information

for *Small*, DOI 10.1002/smll.202404183

Cell Adhesion and Local Cytokine Control on Protein-Functionalized PNIPAM-co-AAc Hydrogel Microcarriers

*Sebastian Bernhard Rauer, Lucas Stüwe, Lea Steinbeck, Marcelo Augusto Szymanski de Toledo, Gereon Fischer, Simon Wennemaring, Jonas Marschick, Steffen Koschmieder, Matthias Wessling and John Linkhorst**

Supporting Information

Cell Adhesion and Local Cytokine Control on Protein-Functionalized PNIPAM-co-AAc Microcarriers

*Sebastian Bernhard Rauer, Lucas Stüwe, Lea Steinbeck, Marcelo Augusto Szymanski de Toledo, Gereon Fischer, Simon Wennemaring, Jonas Marschick, Steffen Koschmieder, Matthias Wessling, John Linkhorst**

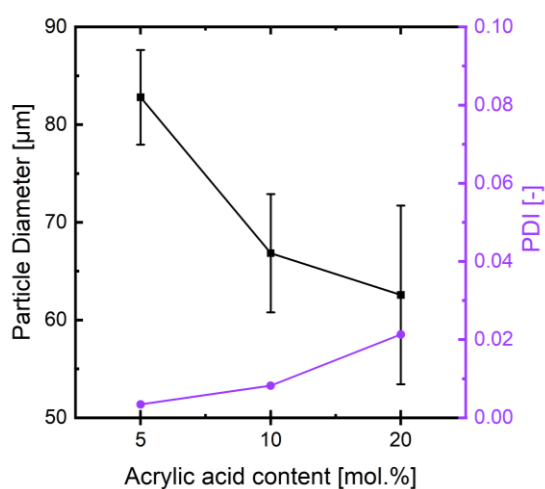


Figure S1. Diameter and polydispersity index (PDI) of PNIPAM-co-AAc microcarriers featuring 10 mol.% BIS crosslinker content and different co-monomer concentrations. The values were calculated from the ImageJ measurement of 150 particles per particle type, each from a single production batch.

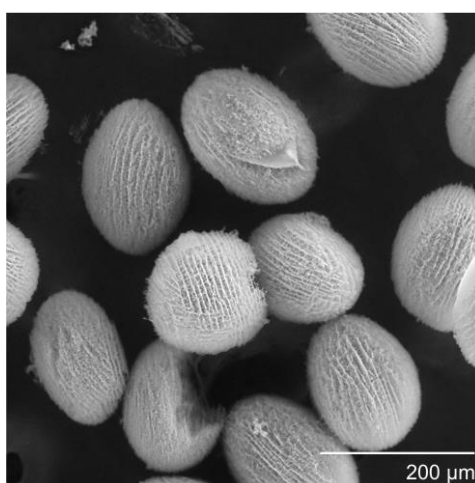


Figure S2. Scanning electron microscopy image of PNIPAM-co-AAc particles featuring a micrometer-sized interconnected porosity generated by freeze-drying.

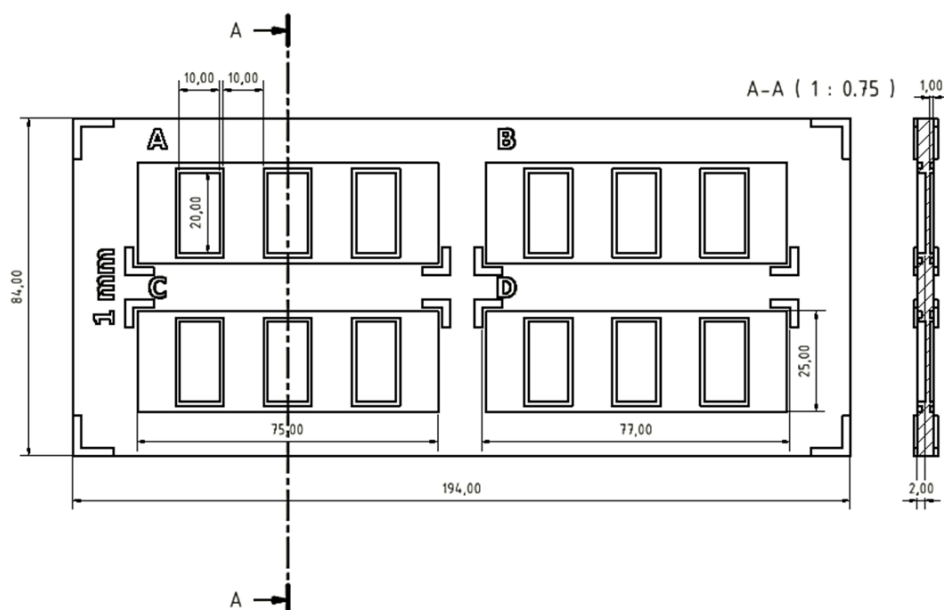


Figure S3. Dimensions of the mold used for the synthesis of PNIPAM-co-AAc films for tensile testing. The mold was fabricated from VeroClear Material (Stratasys) in combination with an Objet Eden 260V (Stratasys) 3D printer. The hydrogel films were UV polymerized from both sides of the mold and featured the dimensions: 20 mm x 10 mm x 1 mm.

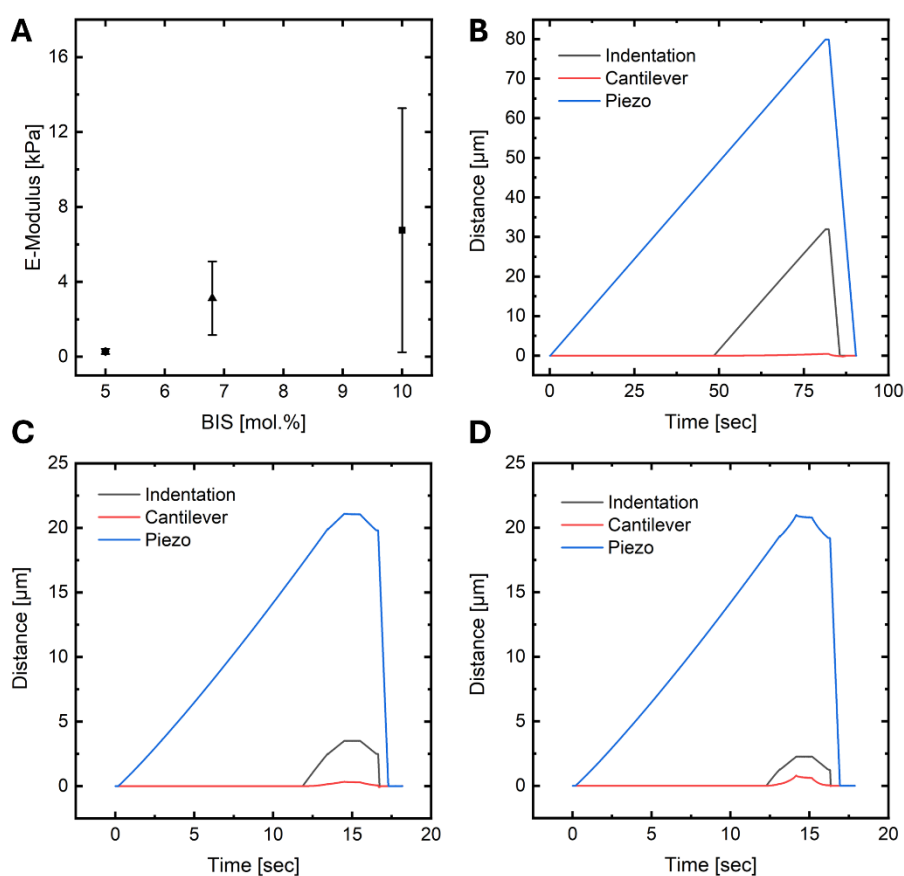


Figure S4. Measurement of local particle elasticity by nanoindentation. A) Effective Young's moduli of spherical PNIPAM-co-AAc particles featuring 5 mol.%, 6.8 mol.%, and 10 mol.% BIS crosslinker content. B) Exemplary measurement sequence for 5 mol.% BIS-containing particles using the displacement mode. C) Exemplary measurement sequence for 6.8 mol.% BIS-containing particles using the indentation mode. D) Exemplary measurement sequence for 10 mol.% BIS-containing particles using the indentation mode; N = 10.

Property	BIS [mol.%]	0 mol.% AAc	10 mol.% AAc	20 mol.% AAc
Zeta Potential	6.8	-1.38 ± 0.28 mV	-17.36 ± 1.52 mV	-26.54 ± 2.44 mV
E-Modulus	5.0	4.08 ± 1.17 [kPa]	4.16 ± 0.63 [kPa]	3.39 ± 0.54 [kPa]
	6.8	7.45 ± 1.98 [kPa]	6.65 ± 1.20 [kPa]	7.47 ± 1.52 [kPa]
	10.0	13.54 ± 1.36 [kPa]	13.13 ± 0.65 [kPa]	13.89 ± 1.39 [kPa]
Fracture Strain	5.0	0.69 ± 0.13 [-]	0.80 ± 0.14 [-]	0.88 ± 0.18 [-]
	6.8	0.54 ± 0.08 [-]	0.64 ± 0.07 [-]	0.65 ± 0.09 [-]
	10.0	0.50 ± 0.07 [-]	0.58 ± 0.05 [-]	0.59 ± 0.10 [-]
Fracture Stress	5.0	2.12 ± 0.74 [kPa]	3.62 ± 1.24 [kPa]	4.25 ± 1.20 [kPa]
	6.8	2.94 ± 0.91 [kPa]	4.00 ± 1.09 [kPa]	4.62 ± 1.06 [kPa]
	10.0	4.78 ± 1.88 [kPa]	5.84 ± 1.26 [kPa]	6.42 ± 2.11 [kPa]

Figure S5. Table summarizing the material properties of PNIPAM-co-AAc hydrogels in dependency of the AAc co-monomer and BIS crosslinker content.

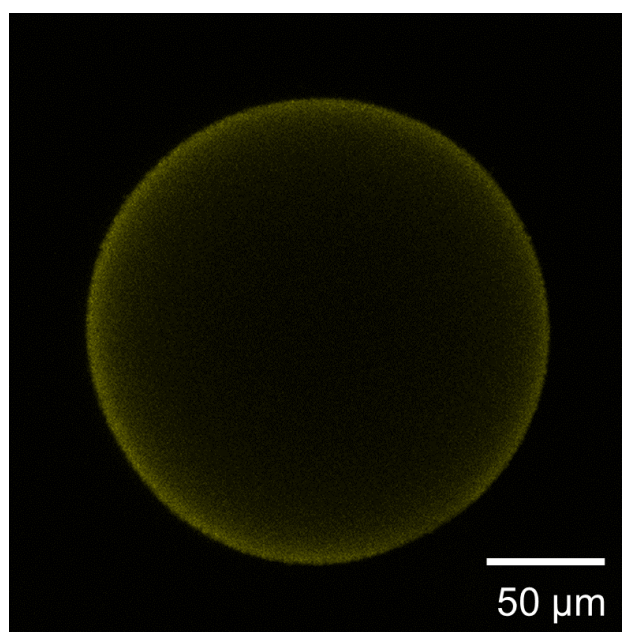


Figure S6. Lucifer Yellow adsorption in the absence of EDC-NHS on pure PNIPAM hydrogel beads.

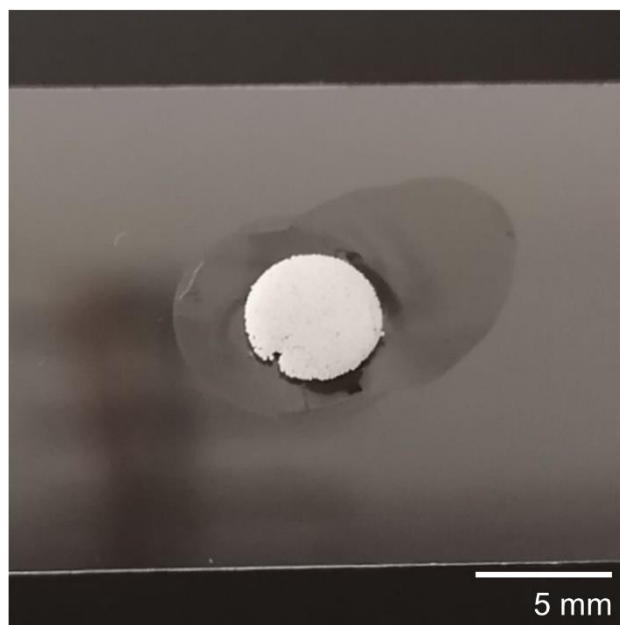


Figure S7. Mechanically stable mm-sized tissue construct formed within 7 days by microtiter-plate cultivations of L929 mouse fibroblasts cells on fibronectin-functionalized PNIPAM-co-AAc microcarriers containing 5 mol.% co-monomer.

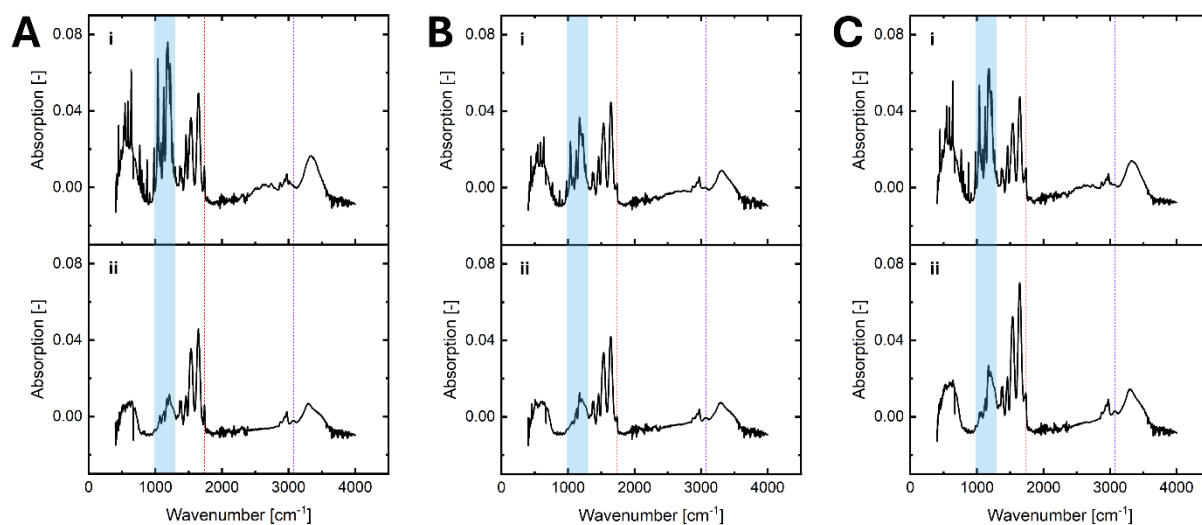


Figure S8. Fourier transform infrared (FTIR) spectroscopy measurements of PNIPAM-co-AAc particles after priming with EDC-NHS (i) and after the subsequent functionalization with gelatin B (ii). A) 5 mol.% AAc-containing particles. B) 10 mol.% AAc-containing particles. C) 20 mol.% AAc-containing particles. For all particle types, the spectra of AAc-NHS depict ester-specific C-O stretching bands between 1000 – 1300 cm^{-1} (blue) and a C=O stretching band at 1740 cm^{-1} (red). Upon conjugation with gelatin B, the C-O stretching bands disappear, while the gelatin-specific amide B band becomes visible at 3080 cm^{-1} (purple), indicating gelatin conjugation.

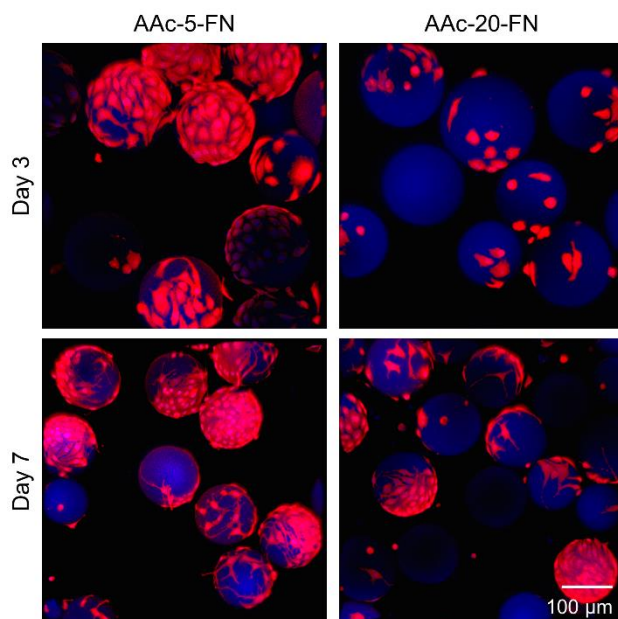


Figure S9. Fluorescence microscopy images of L929 mouse fibroblast cells cultivated on PNIPAM-co-AAc microcarriers functionalized with fibronectin at 10x higher buffer concentration. Activation reaction conditions: $c_{EDC} = 0.2$ M, $c_{NH_2} = 0.2$ M, $pH = 5$, $c_{MES} = 0.5$ M, $t = 20$ min. Coupling reaction conditions: $c_{Gel} = 0.3$ mg/ml, $pH = 5$, $c_{MES} = 0.5$ M, $t = 5$ h. Seeding concentration: $c_{L929} = 200.000$ cells/cm².

Video S10. L929 mouse fibroblast cell adhesion on FN-functionalized PNIPAM-co-AAc microcarriers of 5 mol.% AAc. The video was recorded with a Keyence VHX digital microscope, which illuminates and records the samples from above, which enables the imaging of the upper hemisphere of the microcarriers, on which cells sediment during inoculation.

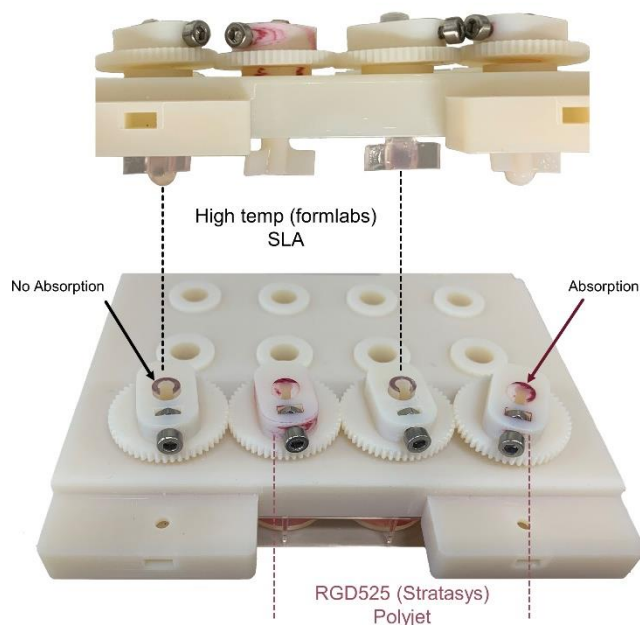


Figure S11. Comparison between polyjet 3D printing (Objet Eden 260V, Stratasys) and stereolithography-based (SLA) 3D printing (formlabs) regarding medium absorption within the printing material. The resulting medium absorption is the result of 24 h incubation in RPMI 1640 medium at 37°C.

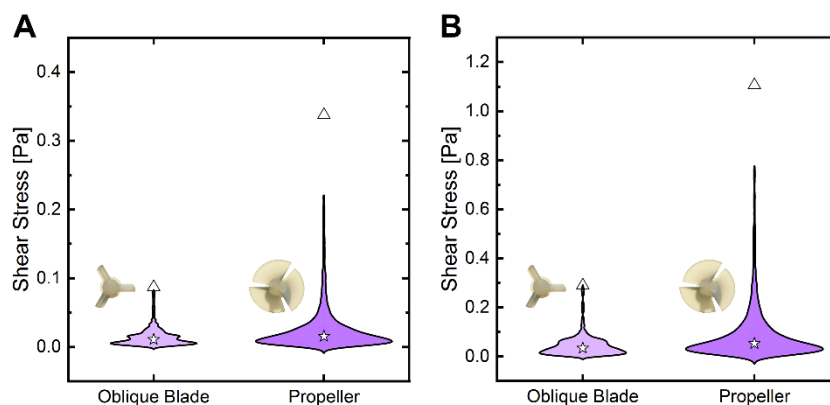


Figure S12. Consol Multiphysics simulation of the shear stress distribution within a compartment of the miniaturized stirred-tank bioreactor (STBR) in dependency of the stirrer geometry and rotational speed at 37°C. A) Cultivation speed: 30 RPM. B) Maximum tested speed: 70 RPM.; symbols: ☆= median, △ = maximum detected value.

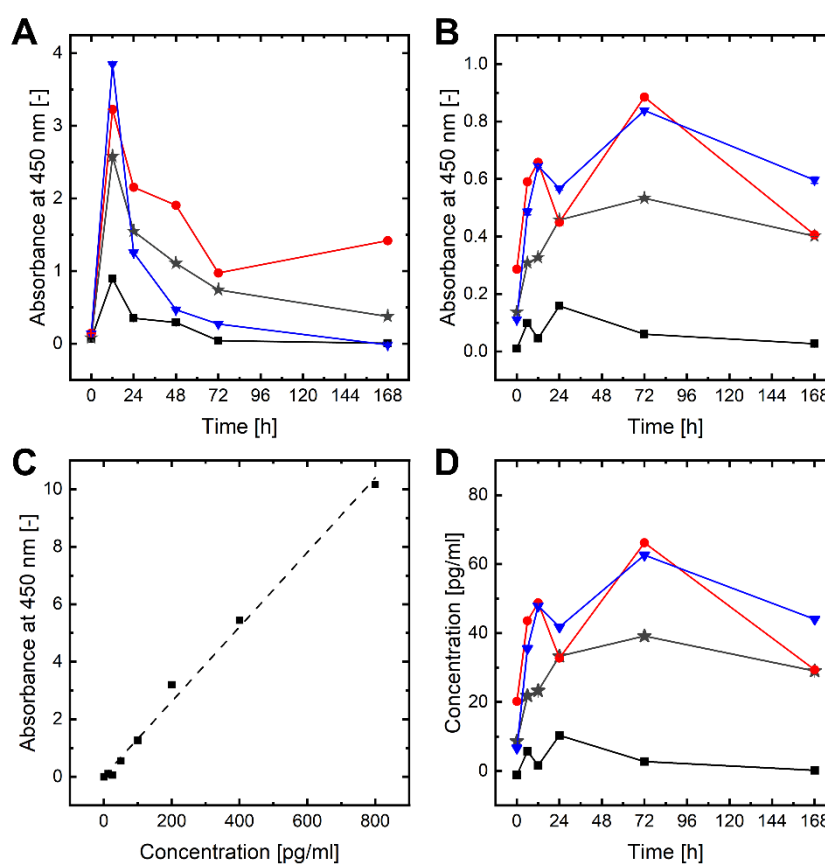


Figure S13. Growth factor (GF) release from adsorptively functionalized microcarriers evaluated by enzyme-linked immunosorbent assays (ELISA) for 0 mol.% AAc (■), 5 mol.% AAc (★), 10 mol.% AAc (●) 20 mol.% AAc (▼). A) Interleukin-3 (IL-3) release in terms of absorbance at 450 nm. B) Vascular endothelial growth factor (VEGF) release in terms of absorbance at 450 nm. C) VEGF calibration curve for the conversion of absorbance to concentration values. D) VEGF release in terms of GF concentration.

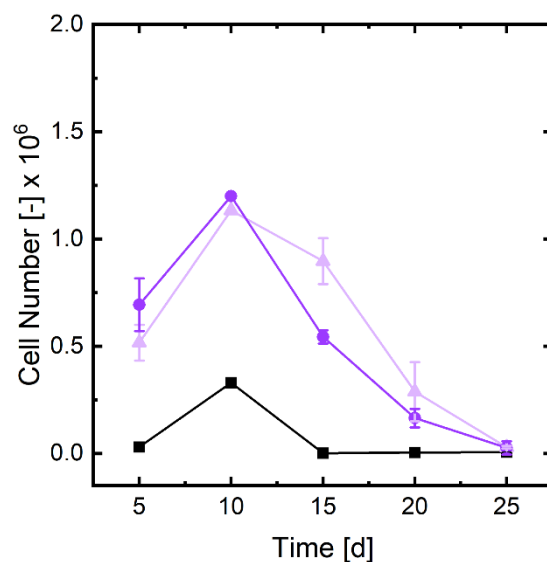


Figure S14. Comparison of non-functionalized (■), adsorptively functionalized (●), and covalently functionalized (▲) microcarriers in terms of cell proliferation in direct contact cultivations. Inoculation concentration in relation to the microtiter plate area: $c = 10.400 \text{ cells/cm}^2$; $N = 3$.

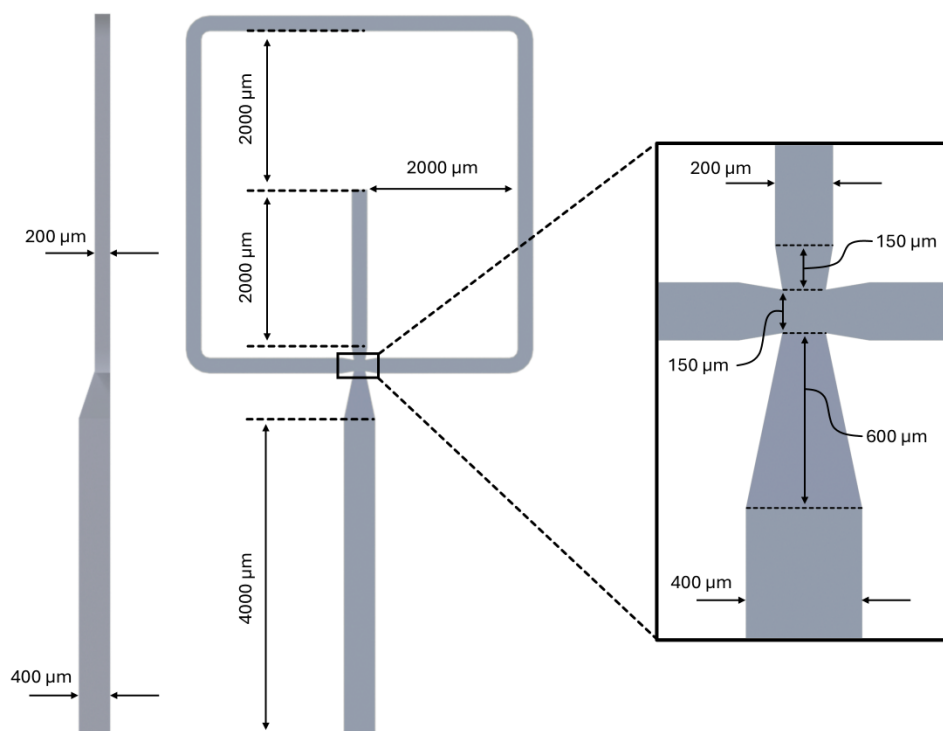


Figure S15. Technical drawing of the microfluidic chip utilized for microcarrier production. The microfluidic device has three identical pre-junction channels which feature a diameter and height of $200 \mu\text{m}$. The diameter decreases to $150 \mu\text{m}$ directly at the junction over $150 \mu\text{m}$, while the height stays constant. The post-junction channel increases in diameter from $150 \mu\text{m}$ to $400 \mu\text{m}$ and in height from $200 \mu\text{m}$ to $400 \mu\text{m}$ over $600 \mu\text{m}$. The droplets travel along the $4000 \mu\text{m}$ long post-junction channel before leaving the chip through the outlet. The distances between the oil-carrying and water-carrying channels were set to $2000 \mu\text{m}$ to simplify the incorporation of inlets and outlet using a biopsy puncher.

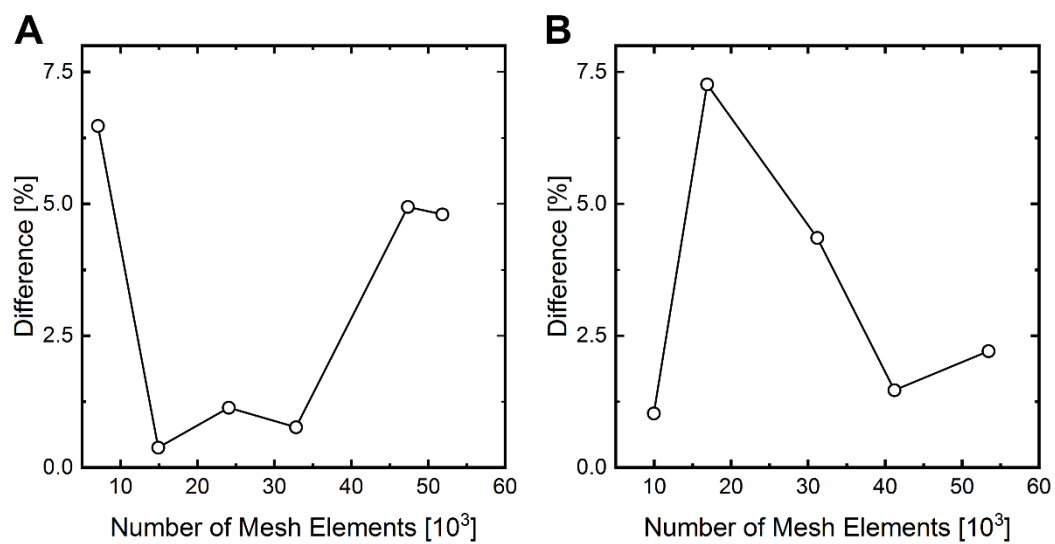


Figure S16. Comsol Multiphysics mesh independence study. A) Oblique blade stirrer. B) Propeller-type stirrer.